Submitted to Physical Review B

LBL-8228
Preprint

QUASIPARTICLE BRANCH MIXING RATES IN SUPERCONDUCTING ALUMINUM

C. C. Chi and John Clarke

September 1978

Prepared for the U. S. Department of Energy
under Contract W-7405-ENG-48

DISCLAIMER

Submitted to Phys. Rev. B

LBL 8228

Quasiparticle Branch Mixing Rates In Superconducting Aluminum

C. C. Chi and John Clarke

Department of Physics, University of California
and Materials and Molecular Research Division
Lawrence Berkeley Laboratory
Berkeley, California 94720

ABSTRACT

The kinetic equation is used to compute the elastic and inelastic quasiparticle branch mixing rates for a superconducting film into which quasiparticles are injected via a tunnel barrier from a second superconducting film. Representative graphs are presented of the steady-state quasiparticle distribution, the quasiparticle charge imbalance, Q^*, vs. injection current, the charge relaxation rate, $\tau_Q^{-1}{}^*$, vs. Δ/k_BT_c for several values of elastic scattering rate, and the quasiparticle branch relaxation rate, τ_Q^{-1}, as a function of energy. The quasiparticle potential developed in the injection film is related to τ_Q^{-1}, and thence to τ_o^{-1}, a characteristic electron-phonon scattering time. Detailed measurements of τ_Q are reported for films of superconducting Al, some of which were doped with oxygen to give a range of transition

temperatures from 1.2 to 2.1K. From the dependence of $\tau_{Q^*}^{-1}$ on $\Delta/k_B T_c$, values are deduced for the gap anisotropy of the films. In the cleanest samples, $\tau_o = 0.10 \pm 0.02\mu sec$, a value that is in good agreement with energy gap relaxation and 2Δ - phonon mean free path measurements, but a factor of about 4 smaller than that obtained from recombination time measurements and theoretical calculations. The value of τ_o^{-1} in the Al films increases with the transition temperature, T_c, as T_c^5 or T_c^6, instead of T_c^3 as predicted by simple theory. It is suggested that the rapid increase of τ_o^{-1} with T_c may arise from either a strong dependence of $\alpha^2 F(\omega)$ on T_c or from a small concentration of magnetic impurities.

I. INTRODUCTION

In a superconducting material, the quasiparticle branch mixing time,[1-3] τ_Q, and quasiparticle recombination time, τ_R, are both proportional to a characteristic time for the electron-phonon interaction, τ_o. The time τ_o is related to T_c, the transition temperature of the superconductor, and to $\alpha^2F(\omega)$, the product of the square of the matrix element of the electron-phonon interaction and the phonon density of states, via the relation[4]

$$\tau_0 = Z_1(0)\hbar[2\pi k_B T_c \alpha^2 F(k_B T_c/\hbar)]^{-1} \qquad (1.1)$$

In Eq. (1.1), $Z_1(0)$ is the real part of the Eliashberg renormalization factor at $\omega = 0$. Provided that the constants of proportionality can be calculated, measurements of either τ_Q or τ_R can be used to estimate τ_o. However, measurements of recombination time often yield a time that is enhanced by phonon trapping.[5] Although one can make estimates of the enhancement factor due to phonon trapping,[6,7] these estimates may be somewhat uncertain because of the difficulty in accurately determining the phonon transmission factor between the sample and the substrate and/or helium bath. On the other hand, measured values of τ_Q are not enhanced by phonon trapping because, for low injection rates, the trapped recombination phonons generate equal numbers of quasiparticles above and below the Fermi wavevector, k_F, so that the branch imbalance is not affected.

Of the several methods[8] of generating and detecting branch imbalance in superconductors, the tunneling injection and detection scheme[1] is

probably the most straightforward. This method was used previously to measure τ_Q in Sn;[9] the results are in good agreement with theoretical estimates.[2,3,4] In this paper, we report measurements of τ_Q in superconducting Al as a function of mean free path and transition temperature. In Section II we first briefly review Tinkham's[3] theory of the generation and detection of branch imbalance, and extend it to the case of a superconducting injection electrode. We next solve the kinetic equation numerically for the injected quasiparticles to find the steady-state distribution and the average branch mixing rate. Representative curves are presented with both inelastic and elastic branch crossing processes, and with inelastic processes alone. Finally in this section, we compute the branch mixing rate as a function of energy, and relate the average value to τ_o^{-1}. In Section III, the experimental techniques are described, and in Section IV the experimental results are presented. For our cleanest films with transition temperatures less than 1.3 K we find $\tau_o = 0.10 \pm 0.02\mu$sec. Measurements of the dependence of τ_o on the transition temperature and the mean free path are reported, and values are deduced for the gap anisotropy of the Al films. Section V contains the discussion and conclusions. First, we compare our value of τ_o with theoretical estimates and other experimental measurements. We then discuss possible explanations for the fact that τ_o^{-1} increases with T_c much more rapidly than the T_c^3 behavior predicted by Eq. (1.1) ($\alpha^2F(\omega)$ is usually quadratic in ω for ω much less than the Debye frequency).

II. THEORY OF BRANCH IMBALANCE

A. Generation and Detection of Branch Imbalance

We briefly review Tinkham's theory of the generation and detection of branch imbalance, and extend it to the case of a superconducting injection electrode. The sample consists of a superconducting film sandwiched between two other metal films with a thin oxide barrier at each interface. Quasiparticles are injected from the injection film, which may be either a normal metal[1,9] or a superconductor (as is the case for the present experiment) into a volume Ω of the middle superconducting film. A normal metal probe (the detector) is coupled to the reverse side of the superconducting film via a second tunnel junction. The detector voltage, V_d, generated between the normal probe and the superconducting film at a point far from the injection region represents the quasiparticle potential, and is measured with a null-balancing technique in which no current flows through the detector junction. V_d is given by [2,3]

$$V_d = Q^*/2N(0)eg_{NS}(0), \tag{2.1}$$

where

$$Q^* \equiv 2N(0)\int_\Delta^\infty [(f_>(E) - f_<(E)]dE. \tag{2.2}$$

In Eqs. (2.1) and (2.2), $N(0)$ is the single-spin electron density of states at the Fermi surface of the superconductor, $g_{NS}(0) = G_{NS}/G_{NN}$ is the ratio of the tunneling conductances of the detector junction in the zero voltage limit with the injected film in the superconducting state and in the normal state, and $f_>(E)$ and $f_<(E)$ are the quasiparticle distribution functions on the $k>k_F$ (denoted by $k_>$) and $k<k_F$ (denoted by

$k_<$) branches. The quantity eQ^* represents the charge imbalance of the quasiparticles. Q^* differs from the quasiparticle population imbalance, Q, by a density of states factor:[2,3]

$$Q \equiv 2N(0)\int_\Delta^\infty \rho_\Delta(E)[f_>(E) - f_<(E)]dE. \qquad (2.3)$$

Here, $\rho_\Delta(E) = E/(E^2 - \Delta^2)^{\frac{1}{2}}$ is the normalized BCS density of states.

In the present experiments the injection film was superconducting with a gap $\Delta' \neq \Delta$. It is straightforward to show that the injection current, I_i, is given by

$$I_i = \frac{G_{NN}}{e}\int_\Delta^\infty \rho_\Delta(E)\{\rho_{\Delta'}(|eV_i - E|)[f(E - eV_i) - f(E)] + \rho_{\Delta'}(eV_i + E)[f(E) - f(E + eV_i)]\}dE, \qquad (2.4)$$

where f(E) is the Fermi function, and G_{NN} is the tunneling conductance of the injection junction with both films in the normal state. The rate of generation of branch imbalance is given by[11]

$$\dot{Q} = \frac{G_{NN}}{e^2\Omega}\int_\Delta^\infty \{\rho_{\Delta'}(|eV_i - E|)[f(E - eV_i) - f(E)] + \rho_{\Delta'}(eV_i + E)[f(E) - f(E + eV_i)]\}dE. \qquad (2.5)$$

In deriving Eqs. (2.4) and (2.5), we have assumed that the departure from thermal equilibrium is small so that we can use the thermal distribution of quasiparticles. This assumption is well-justified in the present work, since the steady-state quasiparticle population never deviated from the thermal equilibrium value by more than 0.05%.[10]

In a steady-state situation, it is convenient to define a quasiparticle charge imbalance relaxation time τ_{Q^*} by[11]

$$\tau_{Q^*} = Q^*/\dot{Q}^*, \qquad (2.6)$$

where $e\dot{Q}^*$, the rate of generation/quasiparticle charge imbalance, is given by[11]

$$\dot{Q}^* = \frac{G_{NN}}{e^2\Omega}\int_\Delta^\infty \rho_\Delta^{-1}(E)\{\rho_{\Delta'}(|eV_i - E|)[f(E - eV_i) - f(E)] + \rho_{\Delta'}(eV_i + E)[f(E) - f(E + eV_i)]\}dE. \quad (2.7)$$

Since both $\dot{Q}$ and $\dot{Q}^*$ are not experimentally measurable quantities, it is convenient to define the two dimensionless parameters[12]

$$F = e\Omega\dot{Q}/I_i, \quad (2.8)$$

$$\text{and } F^* = e\Omega\dot{Q}^*/I_i. \quad (2.9)$$

Both F and F^* can be calculated from Eqs. (2.4), (2.5), and (2.7). In the limit $eV_i >> \Delta, eV_i >> k_BT$, it is easy to show that

$$F \approx 1 - \Delta/eV_i, \quad (2.10)$$

$$\text{and } F^* \approx 1 - \pi\Delta/2eV_i. \quad (2.11)$$

Therefore, /when T is very close to T_c so that $k_BT \gtrsim eV_i >> \Delta$, both F and F^* can be taken as unity without introducing significant errors.

From Eqs. (2.1), (2.6) and (2.9), we find

$$F^*\tau_{Q^*} = 2N(0)g_{NS}(0)\Omega e^2 V_d/I_i. \quad (2.12)$$

All the quantities on the right-hand side of Eq. (2.12) are either experimentally measurable or known constants. One can also relate τ_{Q^*} to the quasiparticle branch mixing time, $\tau_Q \equiv Q/\dot{Q}$, by

$$\tau_Q = F^*\tau_{Q^*}/F(Q^*/Q). \quad (2.13)$$

The value of Q^*/Q depends on the steady-state nonequilibrium distribution functions $f_>(E)$ and $f_<(E)$, and is therefore not as readily obtainable as the factors F and F^*. In order to calculate Q^*/Q, one has either to use

a nonequilibrium model of superconductivity or/compute the steady-state quasiparticle distribution functions from the coupled kinetic equations of the system. We have adopted the latter approach.

B. Calculation of Steady-State Quasiparticle Distribution

In this section, we take $\varepsilon = \pm \sqrt{E^2-\Delta^2}$ as the independent variable, where the plus and minus signs refer to the $k_>$ and $k_<$ branches respectively. The use of the variable ε rather than E avoids the square root singularity of the BCS density of states in the collision integral, and allows for a faster and more accurate computation.

The kinetic equation of the quasiparticles is

$$\dot{f}_\varepsilon = G_\varepsilon - G_{in\varepsilon} - G_{el\varepsilon}. \tag{2.14}$$

G_ε is the quasiparticle generation rate with the injection junction biased at a voltage V_i [11]:

$$G_\varepsilon = R_o\{\tfrac{1}{2}(1 + \tfrac{\varepsilon}{E})[\rho_\Delta'(eV_i - E)\big(1 - f_T(E) - f_T(eV - E)\big)$$

$$+ \rho_\Delta'(E - eV_i)(f_T(E - eV_i) - f_T(E))] - \tfrac{1}{2}(1 - \tfrac{\varepsilon}{E})[\rho_\Delta'(eV_i + E)\times$$

$$(f_T(E) - f_T(eV_i + E)) - \rho_\Delta'(-eV_i - E)(1 - f_T(E) - f_T(-eV_i - E))]\}. \tag{2.15}$$

In Eq. (2.15), $R_o \equiv G_{NN}/2N(0)\Omega e^2$, $E = \sqrt{\varepsilon^2+\Delta^2} > 0$, and $\rho_\Delta \equiv \Theta(E-\Delta)\, E/(E^2-\Delta^2)^{\frac{1}{2}}$, where Θ is the Heaviside function. The thermal distribution function is used in Eq. (2.15) because the departure of the quasiparticle distribution from its thermal equilibrium value is small for our experimental situation.

$G_{in\varepsilon}$ is the collision integral due to inelastic processes:[4]

$$G_{in\varepsilon} = \tau_o^{-1}(k_B T_c)^{-3}\int_{-\infty}^{\infty} d\varepsilon'$$

$$\{\tfrac{1}{2}(1 - \frac{\varepsilon\varepsilon'}{EE'} + \frac{\Delta^2}{EE'})(E + E')^2[f_\varepsilon f_{\varepsilon'} - n_T(E + E')(1 - f_\varepsilon - f_{\varepsilon'})]$$

$$+ \tfrac{1}{2}(1 + \frac{\varepsilon\varepsilon'}{EE'} - \frac{\Delta^2}{EE'})(E - E')^2[\Theta(E - E')(f_\varepsilon - f_\varepsilon f_{\varepsilon'} - n_T(E - E')(f_{\varepsilon'} - f_\varepsilon)$$

$$+ \Theta(E' - E)(-f_{\varepsilon'} + f_\varepsilon f_{\varepsilon'} + n_T(E' - E)(f_\varepsilon - f_{\varepsilon'}))]\}, \qquad (2.16)$$

where $n_T(E) = [\exp(E/k_B T)^{-1}]^{-1}$ is the Bose-Einstein function. Here, we assume that the phonons in the system are in thermal equilibrium at the bath temperature T. Because of phonon trapping,[5] this is not a good assumption if one is interested in the total excess quasiparticle density. However, it is a valid approximation in the calculation of branch imbalance because the trapped excess phonons do not affect the branch imbalance to first order. To further simplify the calculation, the thermal equilibrium gap is used in the kinetic equation. This is also a good approximation for our experimental situation since the maximum deviation of the gap from the thermal equilibrium value is estimated to be less than 1% in the worst possible case over the entire temperature range of interest ($0.8T_c$ to $0.999T_c$).[13] Further, in deriving Eq. (2.16), we have also assumed that $\alpha^2F(\omega)$ can be approximated by $b\omega^2$.

$G_{el\varepsilon}$ is the branch mixing rate of quasiparticles due to elastic processes:

$$G_{el\varepsilon} = \tau_{Qel}^{-1}(E)(f_\varepsilon - f_{-\varepsilon}), \qquad (2.17)$$

where $\tau_{Qel}^{-1}(E)$, the average elastic branch crossing rate of a quasiparticle of energy E, is given by[3]

$$\tau_{Qel}^{-1}(E) = \tau_1^{-1}\langle\rho_\Delta(E)\rho_{\Delta'}(E)[1 - \frac{\Delta\Delta'}{E^2} - (1 - \frac{\Delta^2}{E^2})^{\frac{1}{2}}(1 - \frac{\Delta'^2}{E^2})^{\frac{1}{2}}]\rangle_{\Delta,\Delta'}$$

$$/2\langle\rho_\Delta(E)\rangle_\Delta . \qquad (2.18)$$

Here, τ_1^{-1} is the elastic scattering rate of an electron when the superconductor is in the normal state, and the bracket indicates an average over the gap anisotropy distribution. From Eq. (2.18), it is easy to see that $\tau_{Qel}^{-1}(E) = 0$ if the gap is isotropic, so that gap anisotropy is necessary for elastic scattering to relax branch imbalance. When the gap anisotropy is small, it is convenient to define a root mean square gap anisotropy, $\overline{\delta\Delta}$, by

$$\overline{\delta\Delta} \equiv \langle(\Delta - \overline{\Delta})^2\rangle^{\frac{1}{2}}, \tag{2.19}$$

where $\overline{\Delta} \equiv \langle \Delta \rangle$. For $E >> \overline{\Delta} + \overline{\delta\Delta}$, it can be shown that[14]

$$\tau_{Qel}^{-1}(E) = \tau_1^{-1} \, E \, \overline{\delta\Delta}^2 / 2(E^2 - \overline{\Delta}^2)^{3/2}. \tag{2.20}$$

For $E \lesssim \overline{\Delta} + \overline{\delta\Delta}$, $\tau_{Qel}^{-1}(E)$ can be evaluated exactly from Eq. (2.18) only by using an explicit gap anisotropy distribution function. Fortunately, for the purpose of the branch imbalance calculation, it is sufficient to use Eq. (2.20) for $E \geq \overline{\Delta} + \overline{\delta\Delta}/2$, and $\tau_{Qel}^{-1}(E) = \tau_{Qel}^{-1}(\overline{\Delta} + \overline{\delta\Delta}/2)$ for $E \leq \overline{\Delta} + \overline{\delta\Delta}/2$. The error introduced by making this approximation for $\tau_{Qel}^{-1}(E)$ is of the order of $\overline{\delta\Delta}/\overline{\Delta}$, typically 10^{-3}, for thin superconducting films. Following Markowitz and Kadanoff,[15] we define the normalized mean square gap anisotropy $\langle a^2 \rangle$ by

$$\langle a^2 \rangle \equiv \langle(\Delta - \overline{\Delta})^2\rangle / \overline{\Delta}^2 = \overline{\delta\Delta}^2 / \overline{\Delta}^2. \tag{2.21}$$

For clean bulk superconductors, $\langle a^2 \rangle$ is a constant independent of temperature. For dirty superconductors, for example, thin films, $\langle a^2 \rangle$ is reduced by the Anderson averaging effect[16] from its bulk value, $\langle a^2 \rangle_0$, to[9]

$$\langle a^2 \rangle = \langle a^2 \rangle_o / [1 + (\hbar/2\tau_1\bar{\Delta})^2]$$

$$\approx \langle a^2 \rangle_o (2\tau_1\bar{\Delta}/\hbar)^2, \qquad (2.22)$$

since $(\hbar/2\tau_1\Delta)^2 >> 1$. Then, from Eqs. (2.20) to (2.22), we have

$$\tau_{Qel}^{-1}(E) = \tau_{Qelo}^{-1}(\Delta/k_BT_c)^2 E\Delta^2/(E^2 - \Delta^2)^{3/2}, \qquad (2.23)$$

where τ_{Qelo}^{-1} is defined by

$$\tau_{Qelo}^{-1} = 2\tau_1(k_BT_c)^2\langle a^2 \rangle_o/\hbar^2. \qquad (2.24)$$

For convenience, hereafter we use Δ rather than $\bar{\Delta}$ to represent the average gap.

Since we are mainly interested in the small perturbation limit, we can linearize the kinetic equation, Eq. (2.14), with respect to $\delta f_\varepsilon \equiv f_\varepsilon - f_{T\varepsilon}$. It is easy to see that, in this regime, the steady-state solution of δf_ε scales linearly with the product of the two parameters R_o and τ_o in Eqs. (2.15) and (2.16) respectively. Curves a and b in Fig. 1 are typical examples of our computer calculation of the steady-state solutions for $(\delta f_> - \delta f_<)/R_o\tau_o$. Both curves were calculated for $T/T_c = 0.9$, $V_i = 10\Delta/e$, and $\Delta' = 1.2\Delta$, with $\tau_{Qelo}^{-1}\tau_o = 0$ and 7.8 for curves a and b respectively. Thus, curve a includes inelastic branch mixing only. The addition of elastic branch crossing substantially decreases the branch imbalance near the energy gap, but only slightly affects the branch imbalance at higher energies. These results are expected because $\tau_{Qel}^{-1}(E)$ [Eq. (2.23)] is strongly peaked near the energy gap, and decreases as $1/E^2$ for large E. The commonly-used nonequilibrium model, the chemical potential model,[3] is represented by curve c. This model assumes that

$$\delta f_{\gtrless}(E) = -\frac{\partial f_T(E)}{\partial E}\,\mu_{\gtrless} = \mu_{\gtrless}/4k_BT\cosh^2(E/2k_BT), \qquad (2.25)$$

where $\mu_>$ and $\mu_<$ are the shifted chemical potentials on the two branches. Because $\mu_>-\mu_<$ is an adjustable parameter in the chemical potential model, curve c in Fig. 1 can be shifted up or down to give any desired degree of branch imbalance. However, no position of curve c gives a satisfactory representation of the exact steady-state solution of $\delta f_> - \delta f_<$, especially near Δ. Even in the case of pure inelastic processes (curve a), $\delta f_> - \delta f_<$ has a sharp peak at an energy slightly higher than Δ, while the chemical potential model predicts a sharp peak at Δ (curve c). With the addition of elastic processes (curve b), the peak shifts towards an even higher energy because the quasiparticle branch crossing rates for both inelastic and elastic processes are faster at the energy gap than that at slightly higher energies. The sharp peak at $E = eV_i-\Delta'$ for both curves a and b is due to the BCS density of states of the superconducting injection film. For the case of a normal injection film, this peak disappears as shown by curve a' (broken line in Fig. 1), which was calculated for the same parameters as curve a with $\Delta' = 0$. Below about 7Δ, curves a and a' are indistinguishable.

In the inset of Fig. 1, the calculated Q^* is plotted as a function of injection current, I_i. The solid line and the broken line represent results calculated from families of curves a and a' respectively for various injection voltages, V_i. For large injection voltages ($V_i >> \Delta/e$), the two curves merge together, indicating that the branch

mixing time does not depend on whether the injection film is normal or superconducting. The region of the solid line with zero slope occurs at $V_i \simeq (\Delta + \Delta')/e$, where the injected quasiparticles do not create branch imbalance. The cusp near the origin is due to the cusp in the injection current at $V_i = (\Delta' - \Delta)/e$. The slope of the Q^* vs. I_i curve at large injection voltages gives $F^*\tau_Q^*$, using Eqs. (2.6) and (2.9). Similarly, we have also calculated Q from the steady-state solution of $\delta f_> - \delta f_<$ and $\dot{Q}$ from Eq. (2.5) to obtain the calculated quasiparticle branch mixing time, τ_Q.

In Fig. 2, $(F^*\tau_Q^*)^{-1}\tau_o$ is plotted vs. Δ/k_BT_c for several values of $\tau_{Qelo}^{-1}\tau_o$, while $\tau_Q^{-1}\tau_o$ is shown (broken line) for $\tau_{Qelo}^{-1}\tau_o = 0$. The inset of Fig. 2 shows F, F^*, and Q/Q^* vs. Δ/k_BT_c for $V_i \simeq 10\Delta/e$, and for three values of $\tau_{Qel}^{-1}\tau_o$. F and F^* are independent of $\tau_{Qel}^{-1}\tau_o$, and approximately equal to 0.9 and 0.84 respectively for $\Delta/k_BT_c \gtrsim 0.2$, in agreement with Eqs. (2.10) and (2.11), while Q^*/Q depends strongly on the values of $\tau_{Qelo}^{-1}\tau_o$ and Δ/k_BT_c. However, F, F^*, and Q^*/Q all approach unity as Δ/k_BT_c becomes small. Therefore, for $\Delta/k_BT_c \lesssim 0.2$, there is practically no difference between τ_Q and τ_Q^*, as seen in Fig. 2 for inelastic scattering in the limit $\Delta/k_BT_c \to 0$. Furthermore, all the solid lines tend to the same limit because $\tau_{Qel}^{-1}(E)$ (Eq. 2.20) decreases rapidly as the gap becomes small and only $\tau_{Qin}^{-1}(E)$ is important. It is interesting to note that $\tau_{Qin}^{-1}\tau_o$ is approximately linear in Δ/k_BT_c for $\Delta/k_BT_c \lesssim 0.9$, and can be approximated by

$$\tau_{Qin}^{-1} = 7.2\tau_o^{-1}\Delta/k_BT_c. \qquad (2.26)$$

$(F^*\tau_Q^*{}_{in}^{-1})$ begins to deviate from τ_{Qin}^{-1} when $\Delta/k_BT_c \gtrsim 0.2$. In general,

$(F^{*}\tau_{Q}^{*})^{-1}$ has an upward curvature in $\Delta/k_{B}T_{c}$ that increases as $\tau_{Qelo}^{-1}\tau_{o}$ increases.

C. Inelastic Quasiparticle Branch Crossing Rate

Although it is not necessary to know the inelastic branch crossing rate, $\tau_{Qin}^{-1}(E)$, of a quasiparticle with energy E to obtain the total branch mixing rate, a knowledge of $\tau_{Qin}^{-1}(E)$ gives considerable physical insight. The inelastic collision integral [Eq. (2.16)] contains all the information required to extract $\tau_{Qin}^{-1}(E)$. According to Kaplan, et al.,[4] we have

$$\tau_{Qin}^{-1}(E) = \tau_{o}^{-1}(k_{B}T_{c})^{-3}\{\int_{o}^{\epsilon}d\epsilon'(E-E')^{2}(n_{E-E'} + 1 - f_{E'})(1 - \frac{\Delta^{2}}{EE'} - \frac{\epsilon\epsilon'}{EE'})$$
$$+ \int_{\epsilon}^{\infty}d\epsilon'(E'-E)^{2}(n_{E'-E} + f_{E'})(1 - \frac{\Delta^{2}}{EE'} - \frac{\epsilon\epsilon'}{EE'})$$
$$+ \int_{o}^{\infty}d\epsilon'(E + E')^{2}(n_{E+E'} + f_{E'})(1 + \frac{\Delta^{2}}{EE'} - \frac{\epsilon\epsilon'}{EE'})\}. \quad (2.27)$$

In the limit $E>>\Delta$, $\tau_{Qin}^{-1}(E)$ has the simple asymptotic form

$$\tau_{Qin}^{-1}(E) \approx \tau_{o}^{-1}(k_{B}T_{c})^{-3}E^{2}\Delta\coth(E/2k_{B}T). \quad (2.28)$$

The solid and broken lines in Fig. 3 are the exact $\tau_{Qin}^{-1}(E)$ and their asymptotes respectively for $T = 0.9T_{c}$ and $0.99T_{c}$. One can see that the exact $\tau_{Qin}^{-1}(E)$ does not approach its asymptotic behavior very rapidly. Also, the asymptotic curve fails to show the rise in τ_{Q}^{-1} near Δ, which is partially responsible for the shift of the peak in $\delta f_{>} - \delta f_{<}$ away from Δ in Fig. 1. Because of this increase in $\tau_{Qin}^{-1}(E)$ near Δ, the exact curve crosses its asymptotic curve at a quasiparticle energy not too far away from Δ, so that the asymptotic form of $\tau_{Qin}^{-1}(E)$ [Eq. (2.28)] accidentally gives a fair representation of the exact $\tau_{Qin}^{-1}(E)$ in the whole energy range.

In a steady-state situation, the average branch mixing rate, τ_{Qin}^{-1}, is given by

$$\tau_{Qin}^{-1} = \int_{\Delta}^{\infty}\rho_{\Delta}(E)[\delta f_{>}(E) - \delta f_{<}(E)]\tau_{Qin}^{-1}(E)dE/\int_{\Delta}^{\infty}\rho_{\Delta}(E)[\delta f_{>}(E) - \delta f_{<}(E)]dE. \quad (2.29)$$

Using the exact $\tau_{Qin}^{-1}(E)$ and the steady-state solution of $\delta f_{>} - \delta f_{<}$ found in the previous section, we obtained a result from Eq. (2.29) that was essentially the same as the previous result using the steady-state calculation [Eq. (2.26)]. On the other hand, as in the earlier work of Tinkham,[3] if we use a chemical potential model for the quasiparticle distribution function [Eq. (2.25)] and the asymptotic form for $\tau_{Qin}^{-1}(E)$ [Eq. (2.28)], we find from Eq. (2.29)

$$\tau_{Qin}^{-1} = 4.2\tau_{o}^{-1}\Delta/k_{B}T_{c}. \quad (2.30)$$

The numerical prefactor is surprisingly close to the exact value of 7.2 [Eq. (2.26)].

Using an entirely different approach, namely a linearized version of the Gorkov-Eliashberg equation, Schmid and Schön,[17] and, more recently, Entin-Wohlman and Orbach[18] obtained

$$\tau_{Qin}^{-1} = 6.6\tau_{o}^{-1}\Delta/k_{B}T_{c}. \quad (2.31)$$

The calculation of Schmid and Schön[17] also uses the chemical potential model for the quasiparticle distribution but a different approximation for $\tau_{Qin}^{-1}(E)$[19]:

$$\tau_{Qin}^{-1}(E) = 8.4\tau_{o}\Delta^{2}/E^{2}. \quad (2.32)$$

This approximate form is also shown in Fig. 3 as the dotted line. One can see that it is a good approximation to the exact $\tau_{Qin}^{-1}(E)$ for quasiparticles with energies near the gap where the chemical potential model

predicts the quasiparticle branch imbalance to be a maximum. Therefore, the small difference between Eqs. (2.31) and (2.26) can be attributed to the difference in the steady-state distribution function $\delta f_> - \delta f_<$ obtained from the chemical potential model and the actual steady-state calculation.

Schmid and Schön[17] also considered the case of paramagnetic impurities in the superconductor, and found

$$\tau_{Qin} = \frac{4T}{\pi\Delta}\left(\frac{\tau_E}{2\Gamma}\right)^{\frac{1}{2}}\left(1 + \frac{\hbar^2\Gamma}{2\Delta^2\tau_E}\right)^{\frac{1}{2}}. \tag{2.33}$$

In Eq. (2.33), τ_E, the inelastic scattering time of electrons at the Fermi surface at $T = T_c$, can be related to τ_o by[4]

$$\tau_E = \tau_o/8.4, \tag{2.34}$$

and Γ is given by

$$\Gamma = \tau_s^{-1} + (2\tau_E)^{-1}. \tag{2.35}$$

τ_s is the electron spin-flip time. According to Schmid and Schön[17], Eq. (2.33) is valid if

$$\Delta/k_BT << (\tau_E\Gamma)^{-\frac{1}{2}}. \tag{2.36}$$

When $\tau_s^{-1} = 0$, Eq. (2.33) reduces to Eq. (2.31), and the validity condition [Eq. (2.36)] becomes $\Delta/k_BT << 1.4$ The results of the last section indicate that Eqs. (2.31), and Eq. (2.26) are valid for $\Delta/k_BT \lesssim 1$. Therefore, we suspect that the requirement for the validity of Eq. (2.33) may be too stringent, and that Eq. (2.36) should be replaced by $\Delta/k_BT \lesssim (\tau_E\Gamma)^{-\frac{1}{2}}$. We will return to this point when we discuss our experimental results.

Recently, Chang[20] has calculated $\tau_{Q^*in}(E)$ analytically. His result is

$$\tau_{Q^*in}^{-1}(E) = \tau_o^{-1}(k_B T_c)^{-3}\{\int_o^\infty d\varepsilon'(E-E')^2(n_{E-E'} + 1 - f_{E'})(1 - \frac{\Delta^2}{EE'} - \frac{\varepsilon'^2}{E'^2})$$
$$+ \int_\varepsilon^\infty d\varepsilon'(E'-E)^2(n_{E'-E} + f_{E'})(1- \frac{\Delta^2}{EE'} - \frac{\varepsilon'^2}{E'^2})$$
$$+ \int_o^\infty d\varepsilon(E + E')^2(n_{E+E'} + f_{E'})(1 + \frac{\Delta^2}{EE'} - \frac{\varepsilon'^2}{E'^2})\}. \quad (2.37)$$

In the limit $E>>\Delta$, $\tau_{Q^*in}^{-1}(E)$ can be approximated by:[20]

$$\tau_{Q^*in}^{-1}(E) \approx \frac{\pi}{2}\tau_o^{-1}(k_B T_c)^{-3}E^2\Delta\coth(E/2k_BT). \quad (2.38)$$

The asymptotic value of $\tau_{Q^*in}^{-1}(E)$ [Eq. (2.38)] differs from that of $\tau_{Qin}^{-1}(E)$ [Eq. (2.28)] by a factor of $\pi/2$. In Fig. 4, Chang's values for $\tau_{Q^*in}^{-1}(E)$ and its asymptote are shown for $T = 0.9T_c$ and $0.99T_c$. Again, the asymptotic curves cross the exact curves near Δ. Since $\tau_{Q^*in}^{-1}(E)$ does not rise near the gap energy (as is the case for $\tau_{Qin}^{-1}(E)$), Eq. (2.38) is a reasonable approximation to $\tau_{Q^*in}^{-1}(E)$, especially at temperatures close to T_c.

In a steady-state situation, the average quasiparticle charge relaxation rate, $\tau_{Q^*in}^{-1}$, is defined by

$$\tau_{Q^*in}^{-1} = \int_\Delta^\infty[\delta f_>(E) - \delta f_<(E)]\tau_{Q^*}^{-1}(E)dE/\int_\Delta^\infty[\delta f_>(E) - \delta f_<(E)]dE. \quad (2.39)$$

Equation (2.39) differs from the corresponding equation, Eq. (2.29), for τ_{Qin}^{-1} by the omission of the normalized BCS density of states in the integrals, a factor that is cancelled by the normalized quasiparticle charge. As T approaches T_c, the normalized BCS density of states becomes increasingly less important in the integrals. If the asymptotic forms of $\tau_{Qin}^{-1}(E)$ [Eq. (2.28)] and $\tau_{Q^*in}^{-1}(E)$ [Eq. (2.38)] are used near T_c to obtain their average values, we find $\tau_{Q^*in}^{-1} \approx \frac{\pi}{2}\tau_{Qin}^{-1}$, a result that contradicts the result $\tau_{Q^*in}^{-1} \approx \tau_{Qin}^{-1}$ obtained from the computer calculation.

This contradiction is due to the error introduced by using the asymptotic form for $\tau_{Qin}^{-1}(E)$. If the exact $\tau_{Qin}^{-1}(E)$ [Eq. (2.27)] is used, the factor $\pi/2$ cancels out. For example, using the chemical potential model, Schmid and Schön obtained a better approximation for $\tau_{Qin}^{-1}(E)$ near Δ, so that their result (Eq. 2.31) is a factor $\pi/2$ larger than Tinkham's result [Eq. (2.30)], which used the asymptotic approximation for $\tau_{Qin}^{-1}(E)$.

III. EXPERIMENTAL TECHNIQUES

The sample configuration and experimental procedure were similar to those used by Clarke and Paterson,[9] and are described only briefly here. A typical sample consisted of a 3 × 3 mm Al-AlOx-Al injection junction evaporated onto a glass substrate (inset of Fig. 5). For the "clean" samples, the Al films were evaporated at a typical rate faster than 10nm sec^{-1} from a 5 N Al source in a vacuum better than 10^{-5} torr. For the "intermediate dirty" samples, the Al films were evaporated at rates of between 2 and 10 nm sec^{-1} in a vacuum of 1 to 8 × 10^{-5} torr. For the "dirtiest" samples, oxygen gas was introduced into the evaporation chamber at a steady rate to maintain an oxygen pressure of about 10^{-4} torr and the Al films were evaporated at a rate of 2 to 5nm sec^{-1}. After the injection junction was made, it was masked with a 200-nm thick evaporated film of SiO to produce a 1 × 1 mm window. The second Al film was slightly oxidized, and a diagonal 1-μm thick Cu strip was evaporated to form an Al-AlOx-Cu detector junction.

The detector junction was connected in series with a dc SQUID voltmeter,[21] and the whole circuit was surrounded by a superconducting can to eliminate

external magnetic field fluctuations. The circuit and can were immersed in superfluid liquid helium, the temperature of which could be lowered to about 1 K by means of a diffusion pump. The bath temperature was measured with an Allen-Bradley carbon resistor, and regulated to within ±0.5mK by electrical feedback to a heater in the bath.[22] The detector junction voltage, which varied from 10^{-12} to 10^{-9} V depending on the value of the injection current, was measured with the SQUID voltmeter in a null-current mode. The SQUID was also used to measure the resistance of the detector junction near zero voltage bias. The maximum power generated by the injection current was less than $2Wm^{-2}$.

Table I contains all the essential parameters for the second Al film in the 15 samples reported in this paper. $R_{300}/R_{4.2}$ is the resistance ratio, $\rho_{4.2}$ is the resistivity at 4.2K, and ℓ is the electronic mean free path at 4.2K obtained from the equation[23]

$$\rho_{4.2}\ell = 9 \times 10^{-16}\Omega m^2. \qquad (3.1)$$

R_i is the resistance of the injection junction for $T<T_c$ and $V_i>>(\Delta+\Delta')/e$.

IV. EXPERIMENTAL RESULTS

Figure 5 shows a typical current-voltage characteristic of an injection junction, and the corresponding V_d vs. I_i curve (sample 6 of Table I). The resemblance of this V_d-I_i curve to the theoretical Q^* vs. I_i curve shown in the inset of Fig. 1 is remarkable. The plateau in the V_d vs. I_i curve at $V_i \approx (\Delta+\Delta')/e$ is a direct experimental proof that V_d is proportional to the quasiparticle charge imbalance Q^*.

For some samples, such as the one shown in Fig. 5, there was some asymmetry of the V_d vs. I_i curve about the origin. The degree of asymmetry varied from sample to sample, and was usually more pronounced for samples with small injection resistance, for which the dissipation at a given injection voltage was higher than for samples with a high injection resistance. There was no apparent correlation of the asymmetry with the quality of the injection junction as judged by its current-voltage characteristics. Furthermore, this asymmetry increased at lower temperatures, and disappeared gradually as T approached T_c. The same phenomenon has also been observed for S_n samples.[9] We suspect that the asymmetry arises from the branch imbalance induced by the temperature gradient[24] generated by dissipation in the injection junction. In our measurements, we eliminated this effect by taking the magnitude average of V_d for both polarities of the injection current, I_i.

Figure 6 shows the experimentally measured $(F^*\tau_Q^*)^{-1}$, that is, $I_i\ (2N(0)V_d g_{NS}\Omega e^2)^{-1}$, vs. Δ/k_BT_c for five representative samples. The numbers in parantheses correspond to the sample numbers in Table I. All quantities involved in the experimental data (shown as dots in Fig. 6) were experimentally determined with the exception of N(0), which we took as $1.74 \times 10^{28} eV^{-1}m^{-3}$.[25] The error bars shown in Fig. 6 were mainly due to the uncertainties in the measurements of V_d and Ω. The solid lines were the best fits of the theory described in Sec. II A and B to the data using the two fitting parameters τ_o^{-1} and $\tau_{Qel_o}^{-1}\tau_o$. τ_o^{-1} was determined from the initial slope of the experimental data shown in Fig. 6, and $\tau_{Qel}^{-1}\tau_o$ was determined from the upward curvature needed to fit the data at lower temperatures. The fitting

quality for those samples shown in Fig. 6 is good, and that for the remaining samples was at least comparable. The values of τ_o^{-1} and $\tau_{Qelo}^{-1}\tau_o$ for each sample are listed in Table I. In the last column of Table I. we also list the normalized mean square gap anisotropy $\langle a^2\rangle_o$ in the "clean" limit, which was obtained from Eq. (2.24). For clean bulk Al, both theoretical calculations[26] and experimental results[27] from tunneling measurements of single crystal Al indicate that $\langle a^2\rangle_o \approx 0.01$. Our results for thin Al films are several times larger than this value, and vary widely from sample to sample, with no apparent correlations with $\rho_{4.2}$ or T_c. It should be realized that the values of $\langle a^2\rangle$ in these thin Al films are very small, being reduced from $\langle a^2\rangle_o$ by the factor $(\hbar/2\tau_1\bar{\Delta})^2$[Eq. (2.22)]. Even for the cleanest film we tested, this reduction factor is about 5×10^3 at $0.9T_c$. The remarkable sensitivity of the branch mixing time to small gap anisotropies reflects the weak electron-phonon interaction in Al. A similar degree of gap anisotropy in Sn or Pb could not have a significant effect on τ_Q, as already demonstrated in the work of Clarke and Paterson.[9]

Figure 7 shows the experimentally determined values of τ_o^{-1} vs. T_c. Although there is scatter between different samples with similar T_c's, we see that τ_o^{-1} increases rapidly with T_c. The two straight lines shown in Fig. 7 represent $\tau_o^{-1} \propto T_c^5$ and T_c^6. Now if $\alpha^2F(\omega)$ is more or less independent of T_c, we expect τ_o^{-1} to be proportional to T_c^3 [Eq. (1.1)]. Therefore, our experimental results indicate that as T_c increases from about 1.2 to 2.1 K, either $\alpha^2F(\omega)$ increases substantially, or other branch

relaxation mechanism becomes important. These two possibilities will be further discussed in the next section.

For the cleanest films ($T_c < 1.3K$) we obtained an average τ_o:

$$\tau_o = 0.1 \pm 0.02\mu s \qquad (4.1)$$

at an average T_c of 1.24 K.

V. DISCUSSION AND CONCLUSIONS

Before discussing possible causes for the rapid increase of τ_o^{-1} with T_c, we first compare our value of τ_o for relatively clean films with the values obtained by other workers. Table II lists all the experimental and theoretical values of τ_o for Al known to us. Five values of τ_o have been obtained from measurements of the quasiparticle recombination time, τ_R, using the equation[36]

$$\tau_R^{-1}(T) = \tau_o^{-1}\left(\frac{2\Delta_o}{k_B T_c}\right)^3 \frac{2N_T}{4N(0)\Delta_o}, \qquad (5.1)$$

where N_T, the quasiparticle equilibrium density at temperature T, is given by

$$N_T = 4N(0)\int_\Delta^\infty dE\rho_\Delta(E)/[1 + \exp(E/k_B T)]. \qquad (5.2)$$

Long[31] obtained a value of 0.35μm for the 2Δ- phonon mean free path against pair breaking, Λ, using a technique that avoided enhancement by phonon trapping. We obtained τ_o from Λ using the relationship[37]

$$\tau_o = \left(\frac{2\Delta_o}{k_B T_c}\right)^3 \left(\frac{N_T^2}{2N_{\omega T}}\right)\left(\frac{\Lambda}{v_{ph}}\right)/4N(0)\Delta_o, \qquad (5.3)$$

where $N_{\omega T}$ is the equilibrium density of phonons with energies greater than 2Δ, and v_{ph} is the transverse phonon velocity. Schuller and Gray[34] interpreted

their experimental results using the theory of Schmid and Schön[17] to obtain τ_E, the average inelastic scattering time of electrons at the Fermi surface at $T = T_c$. We converted τ_E to τ_o using Eq. (2.34).

The table is completed by two theoretical estimates of τ_o. Kaplan et al.[4] calculated $\tau_o = 0.44\mu s$ in Al from $\alpha^2[2\Delta(0)]F[2\Delta(0)]$. However, instead of using a measured value of α^2F(which is unavailable), they used the multi-OPW calculations of Tomlinson and Carbotte[38]. Unfortunately, these calculations show considerable scatter for energies below about 1meV, and Kaplan et al.[4] therefore assumed a quadratic energy dependence for α^2F in this region. Thus, their value for τ_o in Al may be less reliable than the value for those metals in which they used a measured form of α^2F. Lawrence and Meador[35] have calculated τ_E^{-1}, the average inelastic quasiparticle scattering rate at the Fermi level, using microscopic theory. They find $\tau_E^{-1} = 1.3 \times 10^7 T^3 s^{-1}$ Using $T = 1.2K$ and $\tau_o = 8.4\ \tau_E$ [Eq. (2.34)], we find $\tau_o = 0.37\mu s$, a value that is in good agreement with the value of $0.44\mu s$ found by Kaplan et al.[4]

The first five entries in Table II have been reviewed in detail by Eisenmenger et al.[39] These authors point out that the measurements of Miller and Dayem[28] and Levine and Hsieh[29] may contain substantial errors because the temperature dependence of the data was not in agreement with theoretical predictions (at low temperatures in the case of Miller and Dayem, and near T_c in the case of Levine and Hsieh). Furthermore, the values of τ_R, and hence of τ_o, contain a phonon trapping enhancement factor that is difficult to estimate with any accuracy. Consequently, we shall not include these two measurements in the subsequent discussion. The remaining experimental values fall into two groups. Group I contains the latest three recombination

time measurements of τ_o that are in good agreement with each other, with an average value of 0.4μs, and also apparently in good agreement with the two theoretical values. However, the agreement of the data of Chi and Langenberg[33] may be somewhat fortuitous. The transition temperatures of their films were about 1.7K, as compared with values of about 1.3K for the films of Gray, et al.[30] and Smith and Mochel,[32] and one would expect the value of τ_o obtained by Chi and Langenberg to be smaller by a factor of about 2.2. Group II contains the estimates of τ_o from the 2Δ - phonon mean free path,[31] the gap relaxation time,[34] and the branch mixing time (present work) with an average value of about 0.1μs that is a factor of four smaller than the theoretical and Group I estimates.

It should also be noted that the theoretical calculations are for bulk, clean aluminum whereas the mean free paths of the Al films on which all of the measurements except our own were made were boundary-limited to a value of the order of 100nm. Schmid[40] has calculated that the inelastic scattering rate for films with a mean free path of 100nm (ρ = 9Ωnm) is roughly three times higher than the rate for bulk aluminum. This increase in the elastic scattering rate arises from the increased coupling between the electrons and the transverse phonons in the presence of impurities. Schuller and Gray[34] used this theory to explain why their value of τ_o obtained in films with mean free paths of 180nm was below the theoretical value. However, our results suggest that this theory may not be valid. In an attempt to compare our results with Schmid's theory, we

have plotted our values of τ_o^{-1} vs. $\rho_{4.2}$ in Fig. 8 (solid circles). The broken line is Schmid's theory (taken from Fig. 4 of ref. 40), with $k_F = 1.75 \times 10^{10} m^{-1}$ [41], and fitted to $\tau_o = 0.40$ s (the average of the two theoretical estimates) in the clean limit ($\rho_{4.2} < 10^{-1} n\Omega m$). It is unreasonable to expect the theory to fit the data for samples in which T_c is significantly higher than the bulk value. Thus, we restrict our comparison of theory and experiment to samples with resistivities below 19nΩm, where T_c ranges from 1.22 to 1.27K. From Fig. 8, it is obvious that the measured τ_o is independent of $\rho_{4.2}$, in this range while the theory predicts that τ_o should change by a factor of about 5. Thus, we conclude that the fact that our value of τ_o for clean Al is a factor of about 4 below the theoretical value cannot be explained by Schmid's theory, and, further, that there is an unresolved discrepancy between the two groups of experimental measurements.

It should be pointed out that the variation of T_c with resistivity in our films is in reasonable agreement with other measurements in the literature. As an example, in Fig. 8 we have plotted the results of Pettit and Silcox[42]

(crosses) together with our own data (open circles). Our transition temperatures are slightly lower, but clearly follow the same trend. It is also noteworthly that, according to the results of Deutscher et al.,[43] the mean free path in the Al films is of the order of the grain size even for our dirtiest films. Thus, the grains are electrically connected, and the resistivity is not due to electron hopping between isolated grains.

We now turn to a discussion of possible mechanisms for the rapid increase of τ_o^{-1} with T_c shown in Fig. 7. One obvious candidate is an increase in the value of $\alpha^2F(\omega) = b\omega^2$. If the form of $\alpha^2F(\omega)$ is independent of T_c, we expect τ_o^{-1} to be proportional to T_c^3 [Eq. (1.1)]. However, as the transition temperature of our samples rises from 1.2 K to 1.8 K, τ_o^{-1} increases by a factor of about 10 (Fig. 7). Thus our data indicate that b must increase by a factor of about 3 over this range of transition temperatures. Now the important contribution of $\alpha^2F(\omega)$ to the scattering is at frequencies $\omega \sim k_BT_c/\hbar$, and our measurements, and the other measurements listed in Table II, are insensitive to the main peaks of $\alpha^2F(\omega)$ located at energies much greater than k_BT_c. Unfortunately, tunneling measurements for Al[44] provide good estimates of $\alpha^2F(\omega)$ only near the peaks, and, to our knowledge, no reliable experimental information is available at low frequencies. However, theoretical calculations[45] on disordered superconductors and experimental measurements[46,47] on disordered Sn and Pb indicate that, at low energies, $\alpha^2F(\omega)$ can not only be substantially greater than for the clean materials, but can also change from a quadratic to a linear dependence on ω. Presumably, similar changes could also occur in Al. Thus, a substantial increase in the low energy part of $\alpha^2F(\omega)$ could explain the rapid increase of τ_o^{-1} with decreasing

mean free path. It is interesting to note, however, that if the frequency dependence becomes linear instead of quadratic, the basic results of our theory will probably not change very much. First, the dependence of τ_Q^{-1} on Δ will not change because this result arises from the properties of the coherence factors. Second, although a linear energy dependence of $\alpha^2F(\omega)$ might lead to a slightly different steady state distribution of quasiparticles, the relaxation rate is always determined by $\alpha^2F(k_BT_c/\hbar)$because the majority of quasiparticles have energies of order k_BT_c for temperatures near T_c. Therefore, if the rapid increase of τ_o^{-1} with T_c is due to an increase in $\alpha^2F(\omega)$, the experimental results lead us to conclude that $\alpha^2F(k_BT_c/\hbar)$for the dirty films is roughly a factor of 6 greater than $\alpha^2F(k_BT_c/\hbar)$for the clean films, irrespective of the form of $\alpha^2F(\omega)$.

We now consider alternative explanations for the rapid increase of τ_o^{-1} with T_c, namely other branch relaxation mechanisms that could also produce a linear dependence of τ_o^{-1} on Δ. A possible candidate is the electron-electron interaction.[48] However, Lawrence and Meador[35] have calculated that the electron-electron scattering rate is only about one-fourth of the electron-phonon rate. Further, in Schmid's calculation[40] plotted in Fig. 8, the rise in τ_o^{-1} for $\rho_{4.2} > 0.3\mu\Omega m$ is largely due to the onset of electron-electron scattering. However, this rate is an order of magnitude lower than the experimentally observed rate. We conclude that electron-electron scattering is unlikely to explain the observed behavior.

According to Eqs. (2.33) and (2.35), another possible mechanism is electron spin-flip scattering by magnetic impurities. It is conceivable that oxygen atoms on the surface and/or at the grain boundaries of the Al films

have dangling bonds with magnetic moments due to the localized unpaired electrons.[49] Such effects have been observed by Witters and coworkers[50] in their measurements of the conduction electron spin resonance of Al. To investigate this possibility, we assume that $\tau_s^{-1} = \eta\ \tau_1^{-1}$, where η is to be determined from the experimental data. In the temperature range of interest ($0.9T_c$ to $0.999T_c$), Eq. (2.33) can be reduced to[51]

$$\tau_{Qin}^{-1} = \frac{\pi\Delta}{4T}\ \tau_E^{-1}(1 + 2\ \tau_s^{-1}/\tau_E^{-1})^{\frac{1}{2}} \qquad (5.4)$$

Therefore, in the presence of an appreciable amount of spin-flip scattering, τ_E^{-1} should be replaced by $\tau_E^{-1}(1 + 2\ \tau_s^{-1}/\tau_E^{-1})^{\frac{1}{2}}$, or, equivalently, τ_o^{-1} should be replaced by $\tau_o^{-1}(T_c)(1 + \tau_s^{-1}/4.2\ \tau_o^{-1}(T_c))^{\frac{1}{2}}$. We further assume that τ_o^{-1} is proportional to T_c^3, so that $\tau_o^{-1}(T_c) = \tau_o^{-1}(1.2K)(T_c/1.2)^3$. Using the relationship between T_c and $\rho_{4.2}$ shown in the inset of Fig. 8, we obtained the solid line in Fig. 8 with $\tau_o^{-1}(1.2K) = 10^7\ s^{-1}$ and $\eta = 4 \times 10^{-7}$. Given the scatter in the data, the fit is quite satisfactory. We note that $(\tau_E\Gamma)^{-\frac{1}{2}}$ is about 1.4 and 1.2 for the cleanest samples and dirtiest sample respectively, while we typically used $\Delta/k_BT \sim 0.2$ to obtain the initial slope in Fig. 6. Thus, we believe that the validity condition [Eq. (2.36)] for Eq. (5.4) is satisfied, particularly in its less restrictive form $\Delta/k_BT \lesssim (\tau_E\Gamma)^{-\frac{1}{2}}$ (see Section II). The conclusion that the increase in τ_o^{-1} may be due to magnetic impurity scattering is obviously very speculative, yet we feel that this mechanism cannot be ruled out. Further light could perhaps be shed on this problem by measuring τ_Q in samples deliberately doped with magnetic impurities.

In summary, for Al samples not deliberately doped with oxygen, we find $\tau_o = 0.10 \pm 0.02\mu sec$ for an average transition temperature of 1.24 K. This result is in good agreement with gap relaxation[34] and 2Δ - phonon lifetime[31] measurements, but roughly a factor of 4 lower than recombination time measurements[30,32,33] and theoretical estimates.[4,35] As the samples are progressively doped with higher concentrations of oxygen, the transition temperature increases, and τ_o^{-1} increases, but at a much faster rate than the expected T_c^3 dependence. This rapid rate of increase of τ_o^{-1} could be explained by an increase in the value of $\alpha^2F(\omega)$, as is known to occur in disordered Sn and Pb films. Alternatively, magnetic impurities could possibly account for the behavior. Finally, the increase in the elastic branch crossing rate as the mean free path is reduced is in good agreement with our computer calculations, which use the anisotropy as a fitting parameter.

ACKNOWLEDGMENTS

We are grateful to J-J. Chang, R. Orbach, and A. Schmid for helpful conversations, and to J-J. Chang, O. Entin-Wohlman and R. Orbach, W. E. Lawrence and A. B. Meador, and J. L. Paterson for preprints of their work. R. Orbach kindly read the manuscript for us. Finally, we are indebted to T. Lemberger and D. Seligson for their measurements on samples 1 to 4.

This work was supported by the Division of Materials Sciences, Office of Basic Energy Sciences, U. S. Department of Energy.

REFERENCES

1. J. Clarke, Phys. Rev. Lett. 28, 1363 (1972).
2. M. Tinkham and J. Clarke, Phys. Rev. Lett. 28, 1366 (1972).
3. M. Tinkham, Phys. Rev. B 6, 1747 (1972).
4. S. B. Kaplan, C. C. Chi, D. N. Langenberg, J-J. Chang, S. Jafarey, and D. J. Scalapino, Phys. Rev. B 14, 4854 (1976).
5. A. Rothwarf and B. N. Taylor, Phys. Rev. Lett. 19, 27 (1967).
6. A. Rothwarf, G. A. Sai-Halasz, and D. N. Langenberg, Phys. Rev. Lett. 33, 212 (1974).
7. W. Eisenmenger, K. Lassmann, H. J. Trumpp, R. Krauss, Appl. Phys. 11, 307 (1976).
8. For an example, see the methods reviewed by D. N. Langenberg: Low Temperature Physics LT 14, (North Holland, Amsterdam, Oxford, and American Elsevier, New York, 1975) M. Krusius and M. Vuorio, Eds. Vol. V, p. 223.
9. J. Clarke and J. L. Paterson, J. Low Temp. Phys. 15, 491 (1974)
10. This upper bound was obtained for the sample with the smallest injection junction resistance (#9 in Table I), with $V_i = 10\Delta/e \approx 1$mV, $T = 0.9\ T_c \approx 1.1$ K, and an assumed average quasiparticle recombination time of 40μsec.
11. J. L. Paterson, unpublished.
12. We have adopted the notation, F, used in Ref. 9, but have replaced the notation used in Ref. 11, G, with F^*.
13. This estimate of 1% was made for sample #9 with $V_i = 10\Delta/e \approx 0.1$mV and $T = 0.999T_c$ using the BCS gap equation with the steady-state distribution function calculated from the kinetic equation. The calculation is not completely self-consistent since the steady-state distribution was calculated using the equilibrium gap.

14. Equation (2.20) differs from Eq. (46) in ref. 3 by a factor of $E/4\sqrt{E^2-\Delta^2}$. A factor ½ comes from the different definitions of $\overline{\delta\Delta}$ ($\overline{\delta\Delta}^2$ in the present paper is $2\overline{\delta\Delta}^2$ defined in ref. 3). A second factor ½ arises from the definition of $\tau_{Qel}^{-1}(E)$, which in the present paper is defined to be the branch crossing rate of a single quasiparticle, while in ref. 3, it referred to the Q-relaxation rate. The factor $E/\sqrt{E^2-\Delta^2}$ arises from the normalized density of final states into which a quasiparticle of energy E can be elastically scattered. Although this factor is unimportant for $E>>\Delta$, in general it should be included for both the branch-crossing and total elastic scattering rates of quasiparticles in superconductors. The inclusion of this factor leads to the usual result that the elastic scattering rate of a quasiparticle of energy E is reduced from the normal state scattering rate, τ_1^{-1}, by a factor $\sqrt{E^2-\Delta^2}/E$.

15. D. Markowitz and L. P. Kadanoff, Phys. Rev. 131, 563 (1963).

16. P. W. Anderson, J. Phys. Chem. Solid 11, 26 (1959).

17. A. Schmid and G. Shön, J. Low Temp. Phys. 20, 207 (1975).

18. O. Entin-Wohlman and R. Orbach, unpublished.

19. The distribution function used by Schmid and Shön [Eq.(5.9) in ref. 17] is essentially the same as that predicted by the chemical potential model except for a factor $N_1(E)/[N_1(E) + 2\Delta\tau_E N_2(E)]$. This factor was also taken to be unity by these authors to obtain their final expression for τ_Q (defined as the transverse relaxation time of the superconducting order parameter in ref. 17). Furthermore, comparing Eq. (5.12) in ref. 17 with Eq. (2.29) in the present paper, we can identify $2\Delta N_2(E)/N_1(E)$ as the equivalent inelastic branch-crossing rate $\tau_{Qin}^{-1}(E)$. Following Schmid and Shön, if we set $N_2(E)/N_1(E) \approx \tau_E^{-1}\Delta/2E^2$ for temperatures near T_c we obtain Eq. (2.32).

20. J-J. Chang, unpublished.

21. J. Clarke, W. M. Goubau, and M. B. Ketchen, J. Low Temp. Phys. 25, 99 (1976).

22. G. I. Rochlin, Rev. Sci. Instrum. 41, 73 (1970).

23. F. R. Fickett, Cryogenics 11, 349 (1971).

24. C. M. Falco, Phys. Rev. Lett. 39, 660 (1977).

25. K. A. Gschneidner, Solid State Phys. 16, 275 (1964)

26. C. R. Leavens and J. P. Carbotte, Can. J. Phys. 49, 724 (1971), and C. R. Leavens and J. P. Carbotte, Ann. Phys. (N.Y.) 70, 338 (1972).

27. B. L. Blackford, J. Low. Temp. Phys. 23, 43 (1976).

28. B. I. Miller and A. H. Dayem, Phys. Rev. Lett. 18, 1000 (1967).

29. J. L. Levine and S. Y. Hsieh, Phys. Rev. Lett. 20, 994 (1968).

30. K. E. Gray, A. R. Long, and C. J. Adkins, Phil. Mag. 20, 273 (1969).

31. A. R. Long, J. Phys. F (Metal Phys.) 3, 2023 (1973).

32. L. N. Smith and J. M. Mochel, Phys. Rev. Lett. 35, 1597 (1976). (We have used the modified value of τ_R as given in ref. 4)

33. C. C. Chi and D. N. Langenberg, Bull. Am. Phys. Soc. 21, No. 3, 403 (1976), and unpublished.

34. I. Schuller and K. E. Gray, Solid State Commun. 23, 339 (1977).

35. W. E. Lawrence and A. B. Meador, unpublished.

36. From the Rothwarf-Taylor equations (Ref. 5), one finds $\tau_R^{-1} = 2N_T R$. It can be shown that $R = \tau_o^{-1}(2\Delta_o/k_B T_c)^3/4N(0)\Delta_o$ at low reduced temperatures. It turns out that Eq. (5.1) is not only an excellent approximation at low reduced temperatures but also in reasonably good agreement with the theoretical calculations of Kaplan et al.(Ref. 4)at temperatures up to 0.9 T_c (C. C. Chi, thesis, Univ. of Pennsylvania, 1976, unpublished).

37. This is the Rothwarf-Taylor relation $RN_T^2 = 2N_{\omega T}/\tau_R$ (ref. 5) with $R = \tau_o^{-1}(2\Delta_o/k_B T_c)^3/4N(0)\Delta_o$ and $\tau_B = \Lambda/v_{ph}$.

38. P. G. Tomlinson and J. P. Carbotte, Solid State Commun. 18, 119 (1976), and private communication (see footnote c of Table I in ref. 4).

39. W. Eisenmenger, K. Lassmann, H. J. Trumpp, and R. Krauss, Appl. Phys. 12, 163 (1977).

40. A. Schmid, Z. Physik, 271, 251 (1974).

41. C. Kittel, Introduction to Solid State Physics, (John Wiley and Sons, New York, 1976), 5th ed., p. 154 .

42. R. B. Pettit and J. Silcox, Phys. Rev. B 13, 2865 (1976).

43. G. Deutscher, H. Fenichel, M. Gershenson, E. Grunbaum, and Z. Ovadyahu, J. Low Temp. Phys. 10, 231 (1973).

44. M. Dayan and G. Deutcher, Low Temperature Physics LT 14, (North-Holland, Amsterdam, Oxford, and American Elsevier, New York, 1975), M. Krusius and M. Vuorio, Eds. Vol. 2, p. 421.

45. G. Bergmann, Phys. Rev. B 3, 3797 (1971).

46. N. V. Zavaritzkii, Zh. Eksperim, i Teor. Fiz. 57, 752 (1969) [Sov. Phys. JETP 30, 412 (1970)].

47. K. Knorr and N. Barth, Solid State Commun. 8, 1085 (1970).

48. D. C. Lancashire, J. Phys. F: (Metal Phys.) 2, 107 (1972).

49. It has been shown that such dangling bonds can occur in the microcracks of Si and Ge or in amorphous Si and Ge. See B. P. Lemke and D. Haneman, Phys. Rev. B 17, 1893 (1978).

50. J. Witters, private communication through R. Orbach, and A. Stesmans, J. van Meijel, and J. Witters, Solid State Commun. 21, 705 (1977), J. R. Sambles, J. E. Cousins, A. Stesmans, and J. Witters, Solid State

Commun. 24, 673 (1977).

51. The factor $(1 + \hbar^2\Gamma/2\Delta^2\tau_E)^{\frac{1}{2}}$ in Eq. (2.33) is very close to 1: Γ is estimated to be less than $2 \times 10^8 \text{sec}^{-1}$, and $\hbar^2\Gamma/2\Delta^2\tau_E \sim 5 \times 10^{-14}\Gamma$ at $T = 0.999T_c$.

Table I. Measured and calculated quantities for the eleven samples tested.

Sample	Film Thickness (nm)	T_c (K)	$\frac{R_{300}}{R_{4.2}}$	$\rho_{4.2}$ (rΩm)	ℓ (nm)	R_i (Ω)	τ_o (ns)	$\tau_{Qelo}^{-1}\tau_o$	$\langle a^2\rangle_o$ [a]
1	590	1.219	13.7	2.2	409	0.70	97		
2	560	1.219	13.9	2.3	391	0.40	95		
3	590	1.226	14.0	2.4	375	0.46	90		
4	566	1.217	12.6	2.8	317	0.54	100	20.8	0.022
5	210	1.228	5.1	9.0	100	0.13	90	7.8	0.034
6	200	1.231	5.1	9.0	100	0.32	102	13.0	0.049
7	244	1.262	4.8	10.0	90	0.65	108	5.2	0.020
8	275	1.267	3.7	11.5	78	1.22	111	5.2	0.022
9	206	1.253	3.0	17.0	53	0.067	120	3.9	0.023
10	95	1.241	3.9	19.0	49	2.1	66	5.2	0.076
11	126	1.306	2.6	39.0	23	0.20	67	0.78	0.017
12	110	1.411	2.5	72.0	12.5	0.80	49	0.52	0.025
13	190	1.573	1.7	150	6.0	0.46	13	0.26	0.079
14	130	1.886	1.1	800	1.1	4.0	10	< 0.1	< 0.15
15	130	2.113	1.0	850	1.0	2.0	8.5	< 0.1	< 0.18

[a] The uncertainties in $\langle a^2\rangle_o$ arise from the uncertainties in the curve fitting used to determine $\tau_{Qel}^{-1}(0)\tau_o$. For samples 14 and 15 the upward curvature is so small that only an upper bound on $\langle a^2\rangle_o$ can be given. For samples 1 to 3 measurements were taken only within 10mK of T_c, so that values of $\tau_{Qelo}^{-1}\tau_o$ and $\langle a^2\rangle_o$ were not determined.

Table II. Values of τ_o for aluminum

Authors	Quantity Measured	T_c(K)	phonon trapping enhancement factor	τ_o (μ sec.)
Miller and Dayem[28]	Effective recombination time	1.45		1.1
Levine and Hsieh[29]	Effective recombination time	1.2		0.2
Gray, Long, and Adkins[30]	Effective recombination time	1.3	7	0.36
Long[31]	2Δ - phonon mean free path (Λ = 0.35μm)	1.3	1	0.10
Smith and Mochel[32]	Intrinsic recombination time (T_R = 1.4μs at Δ/k_BT = 6)	1.3	1	0.44
Chi and Langenberg[33]	Effective recombination time (τ_{Reff} = 0.03μs at Δ/k_BT = 1.5)	1.7	1.1	0.39
Schuller and Gray[34]	Gap relaxation time	1.21	1	0.13
Present work	Branch mixing time	1.25	1	0.10
Kaplan, et al.[4]	(Calculated)	1.2	-	0.44
Lawrence and Meador[35]	(Calculated)	1.2	-	0.37

Figure Captions

Fig. 1. Computed branch imbalance in the quasiparticle distributions vs. energy for a 100 nm- thick film with Δ = 0.1meV, with quasiparticles injected from a second film with Δ' = 0.12meV through a 1Ω - 3mm × 3mm tunnel junction biased at 1mV. Curves a and b were calculated from the coupled kinetic equations with $\tau_{Qelo}^{-1}\tau_o$ = 0 and 7.8. Curve a' was calculated for $\tau_{Qelo}^{-1}\tau_o$ = 0 with Δ' = 0. Curve c is the prediction of the chemical potential model.

Fig. 2. Calculated values of $(F^*\tau_{Q^*})^{-1}\tau_o$ vs. $\Delta(T)/k_BT_c$ for eight values of $\tau_{Qelo}^{-1}\tau_o$: 0, 0.65, 1.3, 2.6, 5.2, 7.8, 13, 20.8. $\tau_{Qin}^{-1}\tau_o$ (broken line) is shown for comparison. Insert shows Q^*/Q (solid lines) for $\tau_{Qelo}^{-1}\tau_o$ = 0, 2.6, 20.8, and F (broken line) and F^* (dotted line), which are independent of the value of $\tau_{Qelo}^{-1}\tau_o$.

Fig. 3. Inelastic quasiparticle branch mixing rates, $\tau_Q^{-1}(E)\tau_o$, vs. quasiparticle energy E/Δ_o obtained from the exact equation, Eq. (2.27) (solid line), and two different approximations, Eq. (2.28) (broken line), and Eq. (2.32) (dotted line).

Fig. 4. Inelastic quasiparticle charge imbalance relaxation rates, $\tau_{Q^*}^{-1}\tau_o$, vs. quasiparticle energy E/Δ_o obtained from the exact equation, Eq. (2.37) (solid line) and an approximate form, Eq. (2.38) (broken line).

Fig. 5. Measured V_i and V_d vs. I_i for sample 6. Note the two different voltage scales. Inset shows sample configuration.

Fig. 6. Measured values of $(F^{*}\tau_{Q}^{*})^{-1} = I_i/2N(0)g_{NS}(0)\Omega eV_d$ vs. $\Delta(T)/k_BT_c$ for 5 of the samples listed in Table I (sample numbers shown in paranthesis).

Fig. 7. τ_o^{-1} vs. T_c for Al films. The two solid lines, representing T_c^5 and T_c^6 dependences, while the broken line represents a T_c^3 dependence.

Fig. 8. Experimentally determined τ_o^{-1} (left hand ordinate) vs. measured residual resistivity $\rho_{4.2}$ (●). Broken line is the theoretical calculation of Schmid (Ref. 40). Solid line represents $\tau_o^{-1}(T_c)[1 + \eta\tau_1^{-1}/4.2\pi\tau_o^{-1}(T_c)]^{\frac{1}{2}}$ (right hand ordinate). Inset shows the measured T_c vs. $\rho_{4.2}$ for the present experiment (o) together with data taken from Ref. 42 (x).

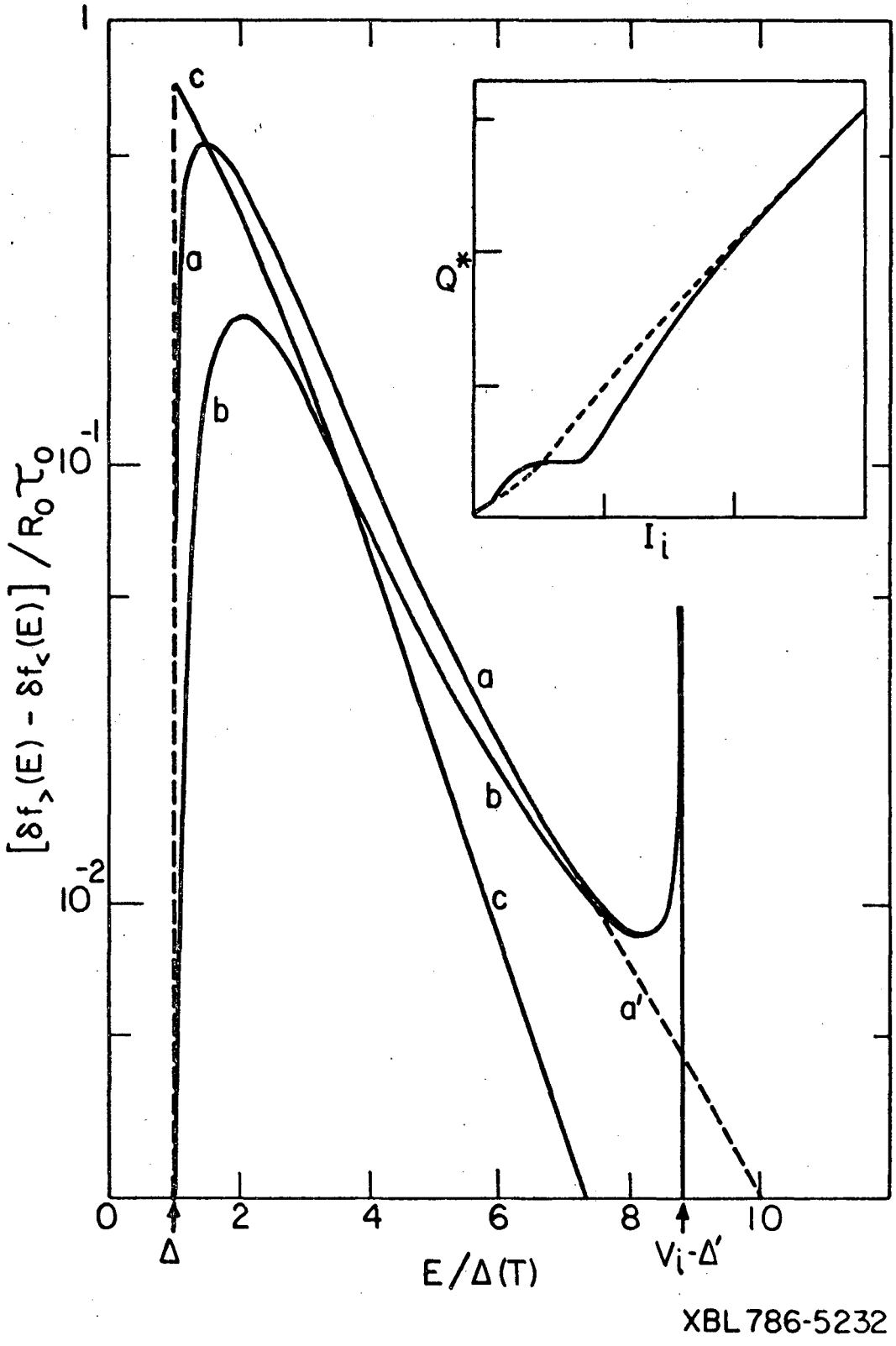
1
10^{-1}
10^{-2}
$[\delta f_>(E) - \delta f_<(E)] / R_0 \tau_0$
c
a
b
Q*
I_i
a
b
c
a'
0
2
4
6
8
10
Δ
$E/\Delta(T)$
$V_i - \Delta'$
XBL 786-5232

Fig. 1

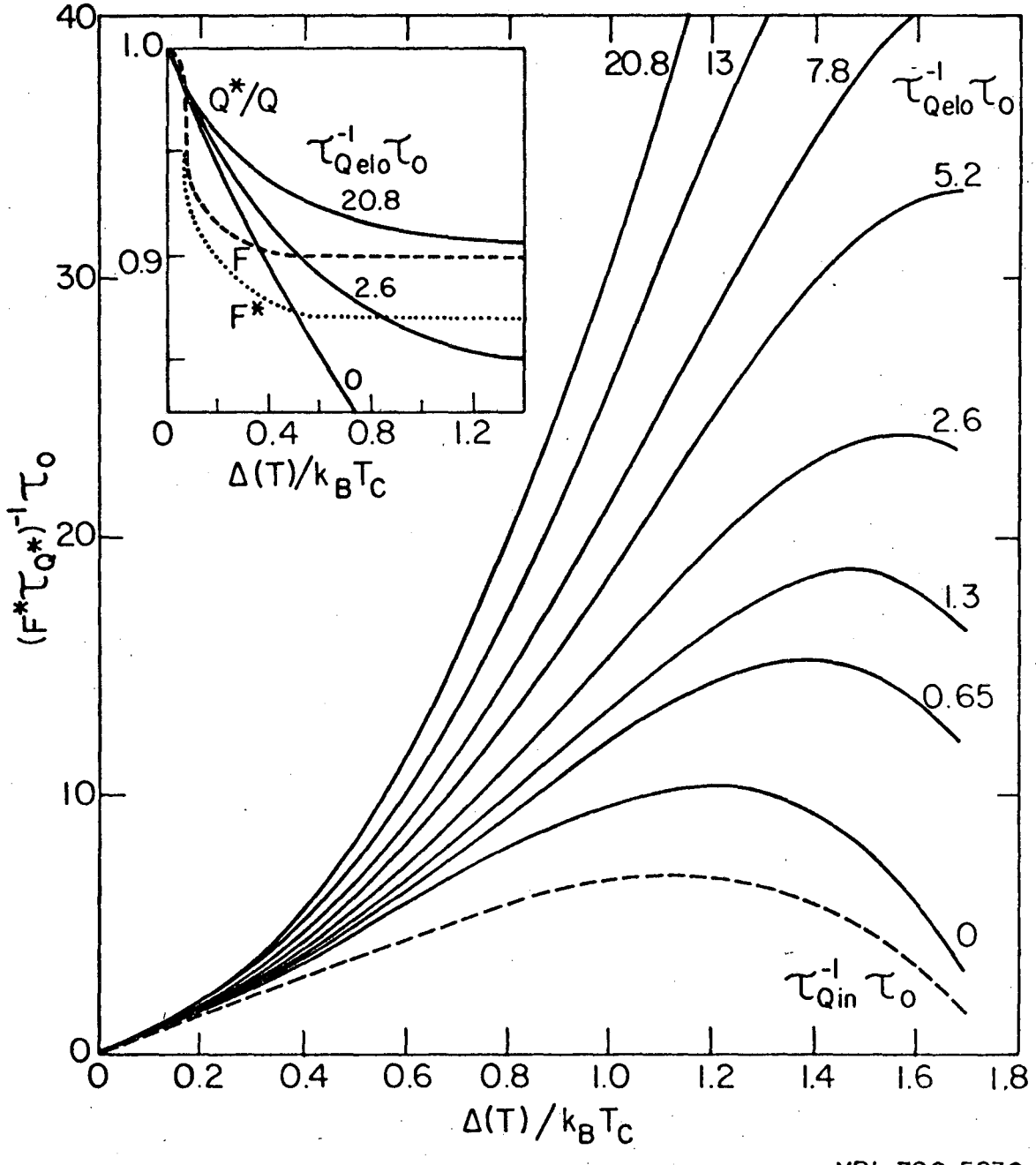

XBL 786-5230

Fig. 2

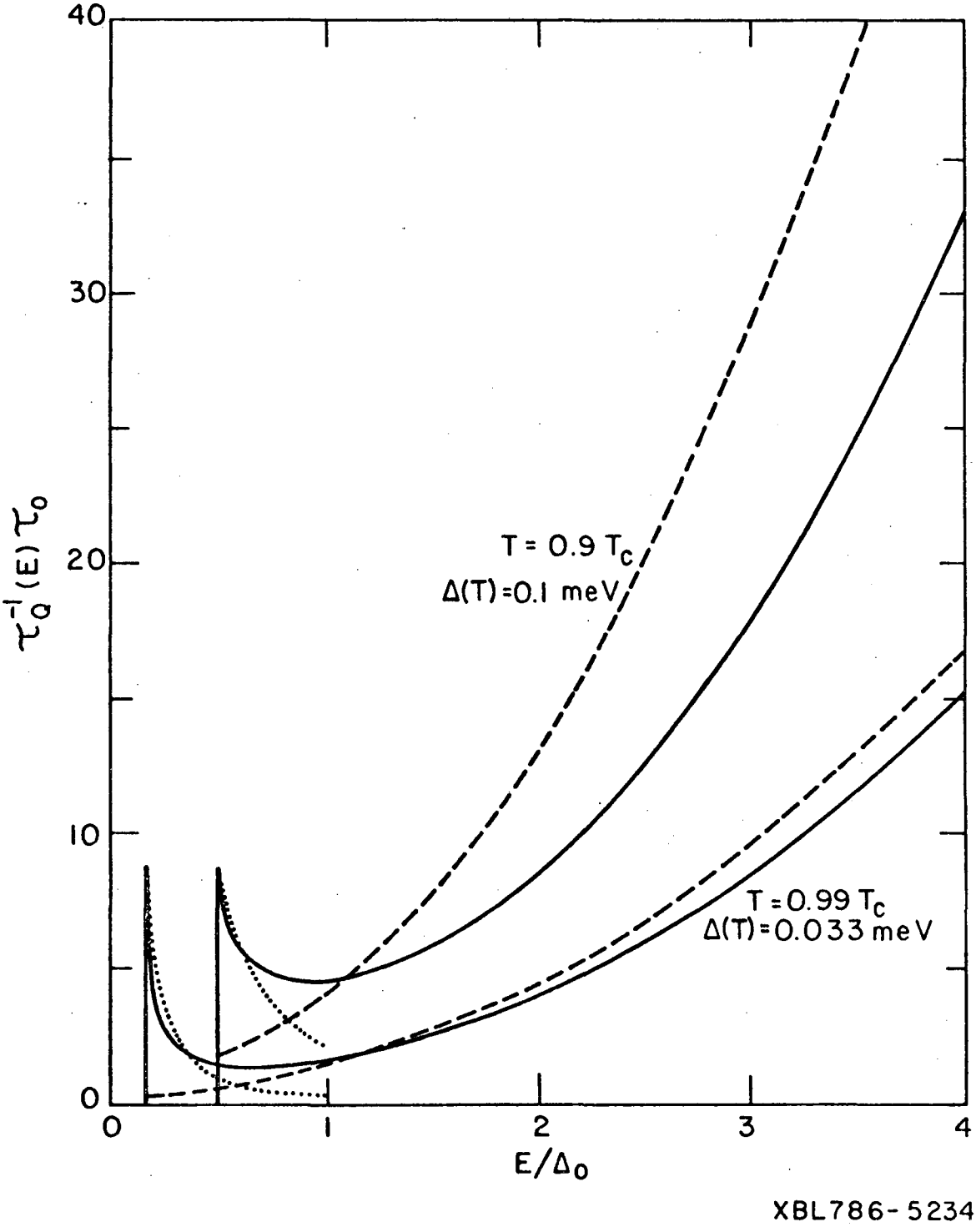
40
30
20
10
0
0
1
2
3
4
$\tau_0^{-1}(E)\tau_0$
E/Δ_0
T = 0.9 T_c
Δ(T)=0.1 meV
T = 0.99 T_c
Δ(T)=0.033 meV
XBL786-5234

Fig. 3

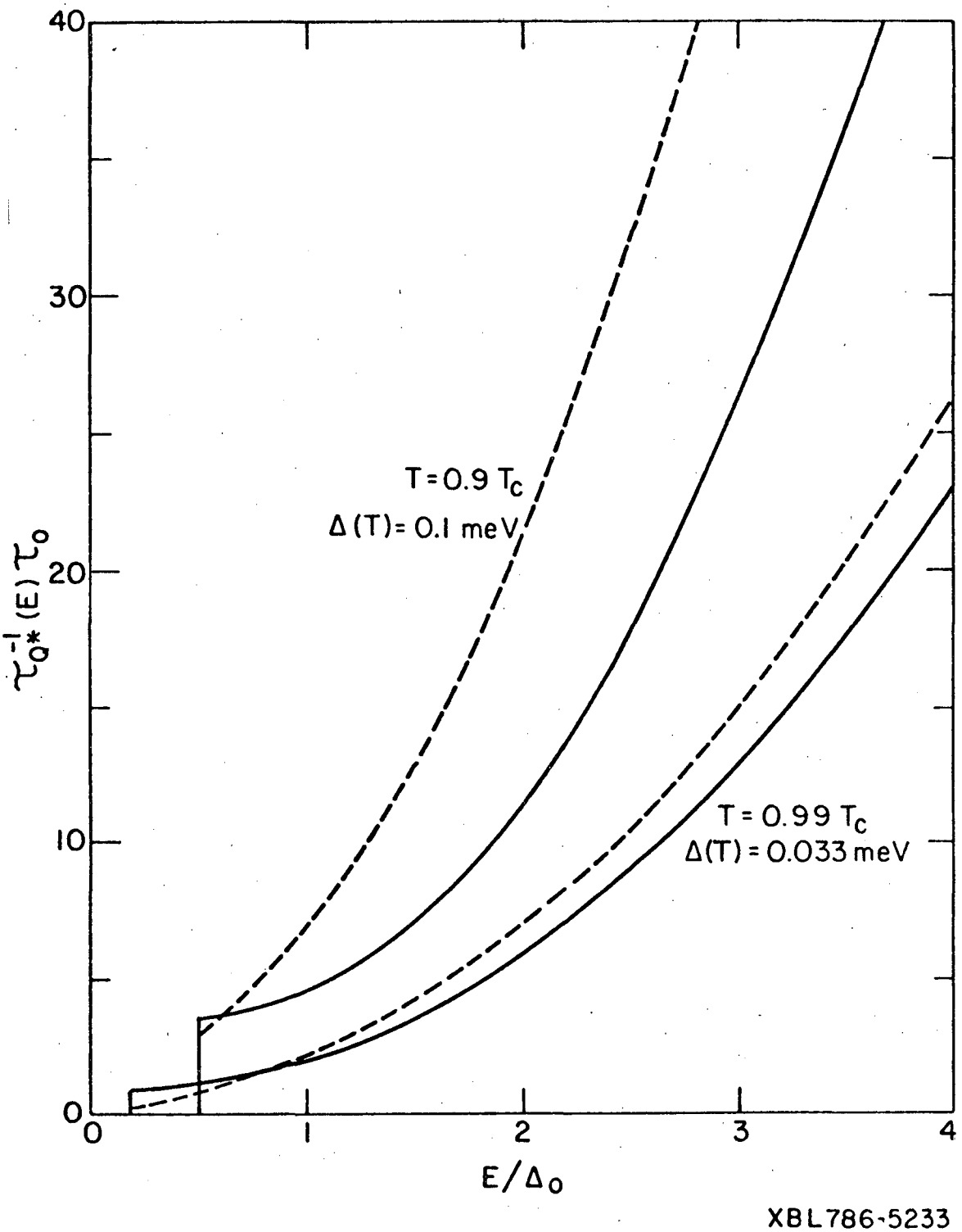
40
30
20
10
0
0
1
2
3
4
$\tau_0^{-1}(E)\tau_0$
E/Δ_0
T = 0.9 T_c
Δ(T) = 0.1 meV
T = 0.99 T_c
Δ(T) = 0.033 meV
XBL786-5233

Fig. 4

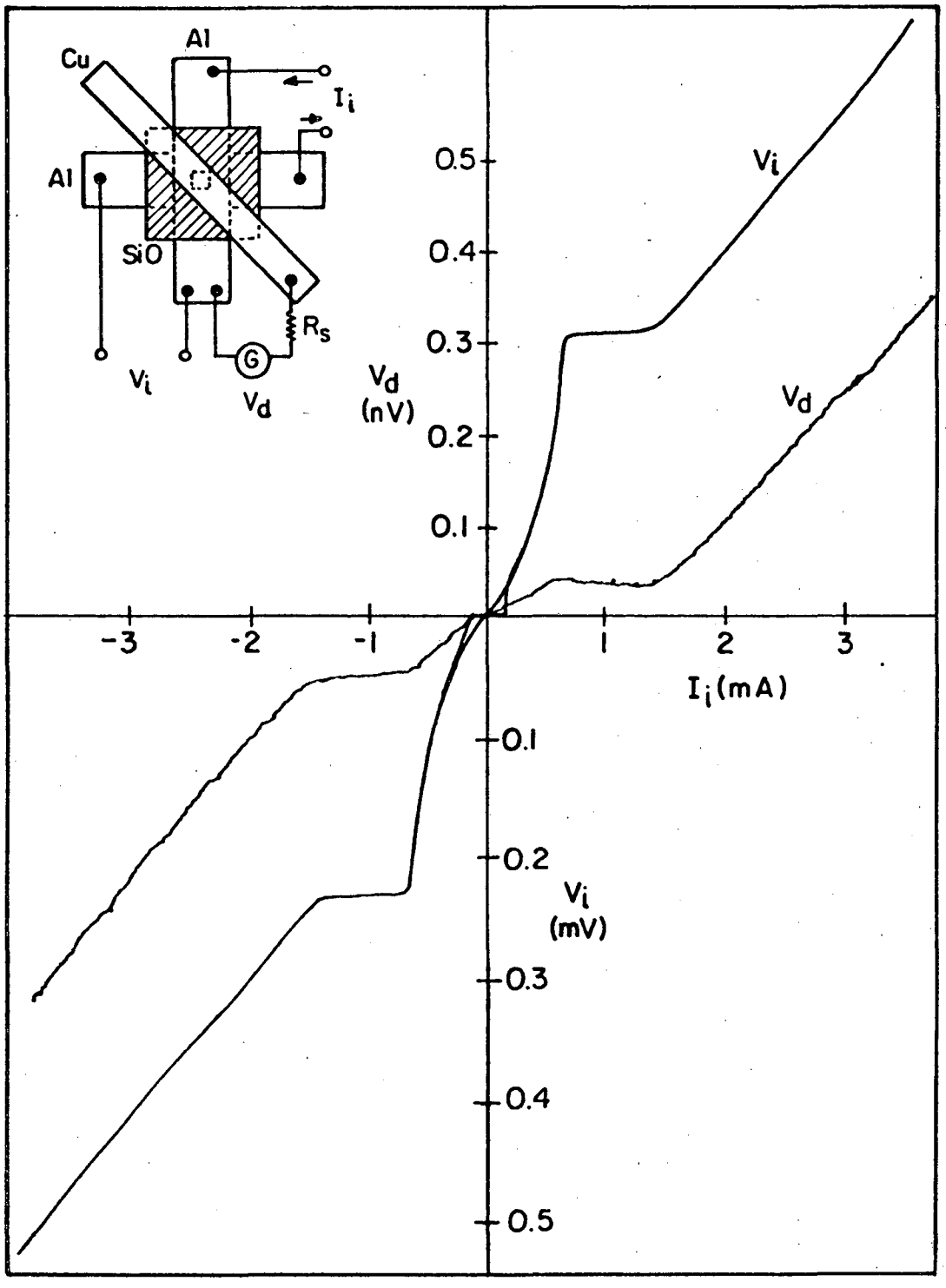

XBL 7710-6152

Fig. 5

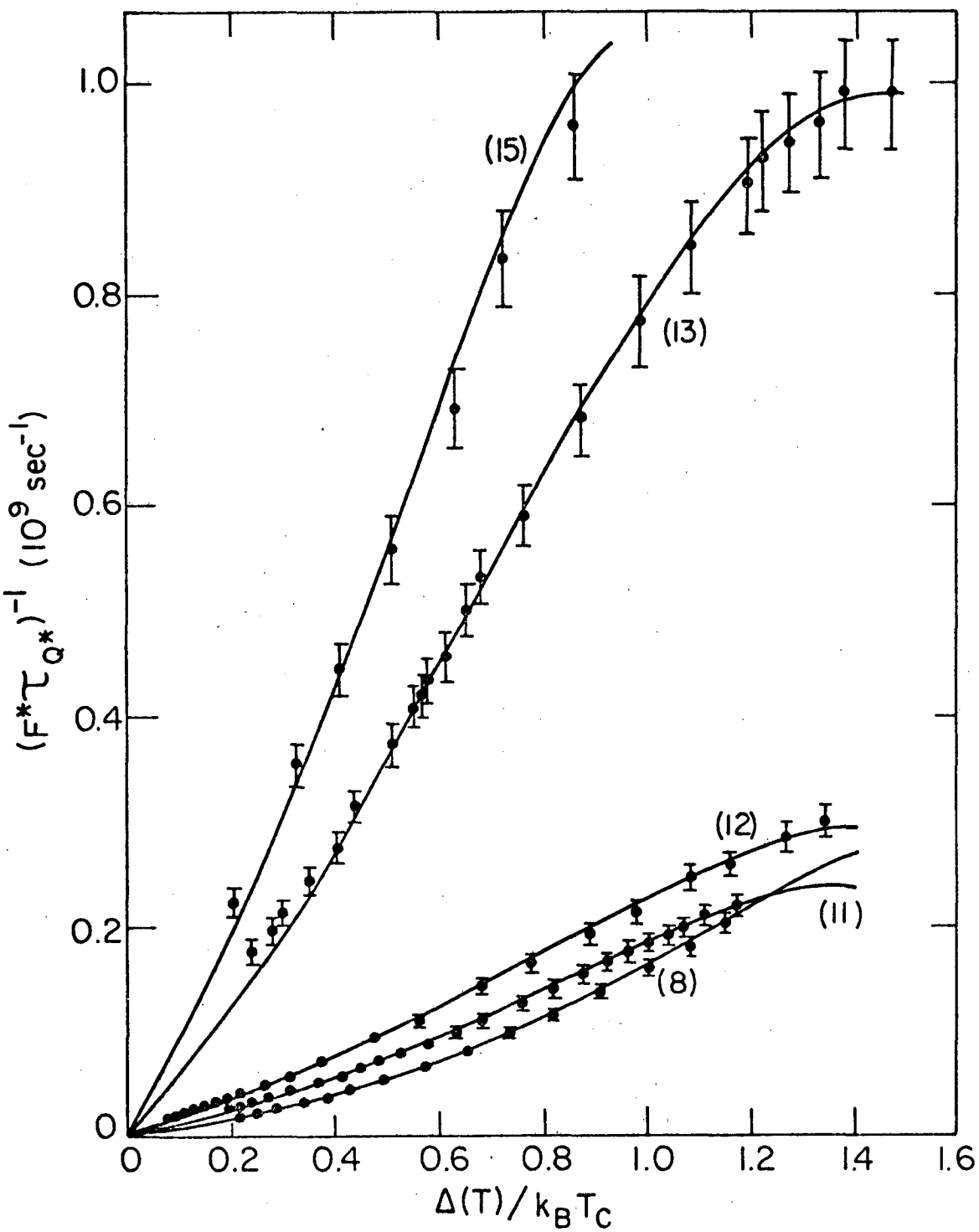

XBL 786-5235

Fig. 6

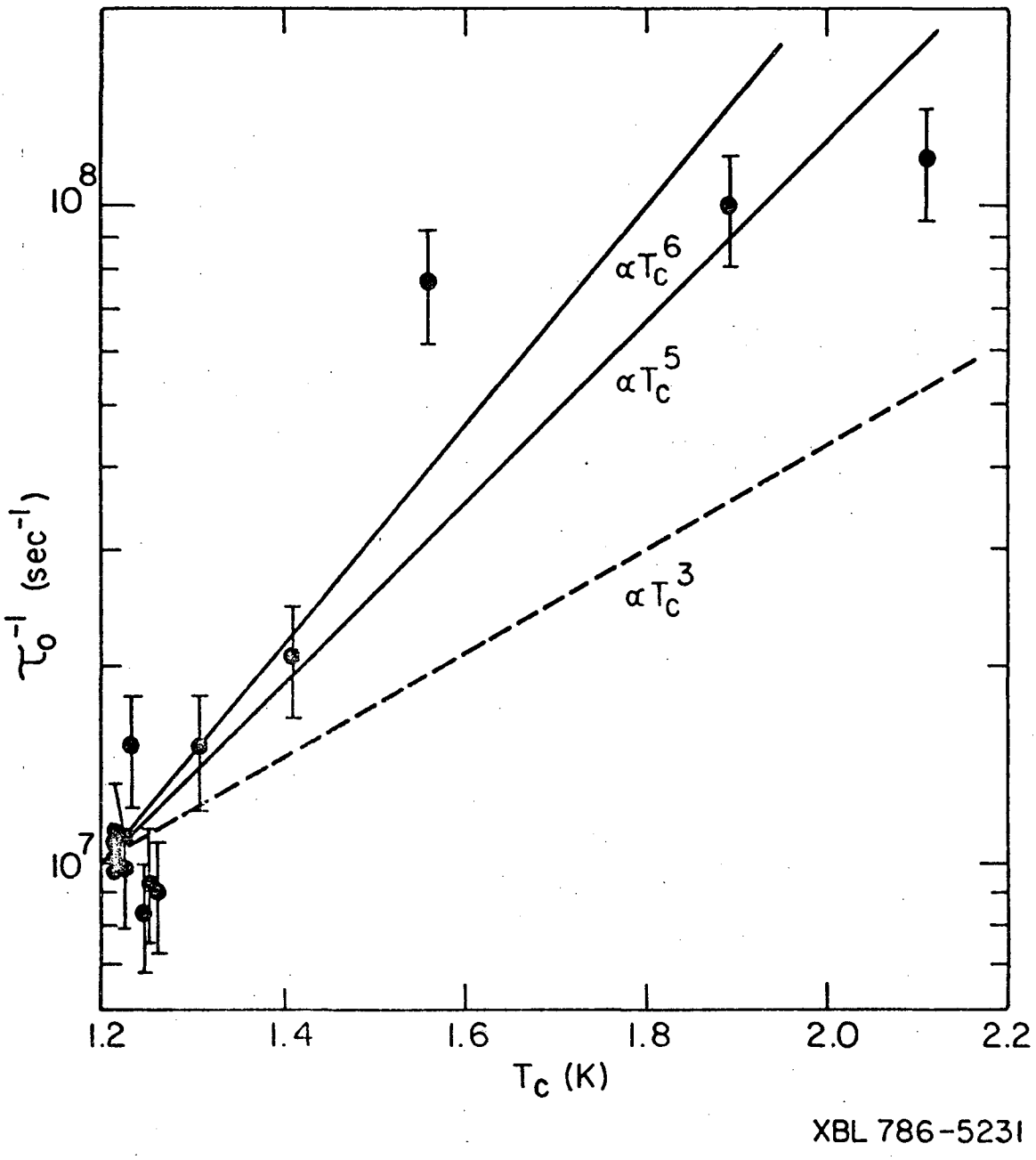
10^8
10^7
τ_0^{-1} (sec^{-1})
$\propto T_c^6$
$\propto T_c^5$
$\propto T_c^3$
1.2
1.4
1.6
1.8
2.0
2.2
T_c (K)
XBL 786-5231

Fig. 7

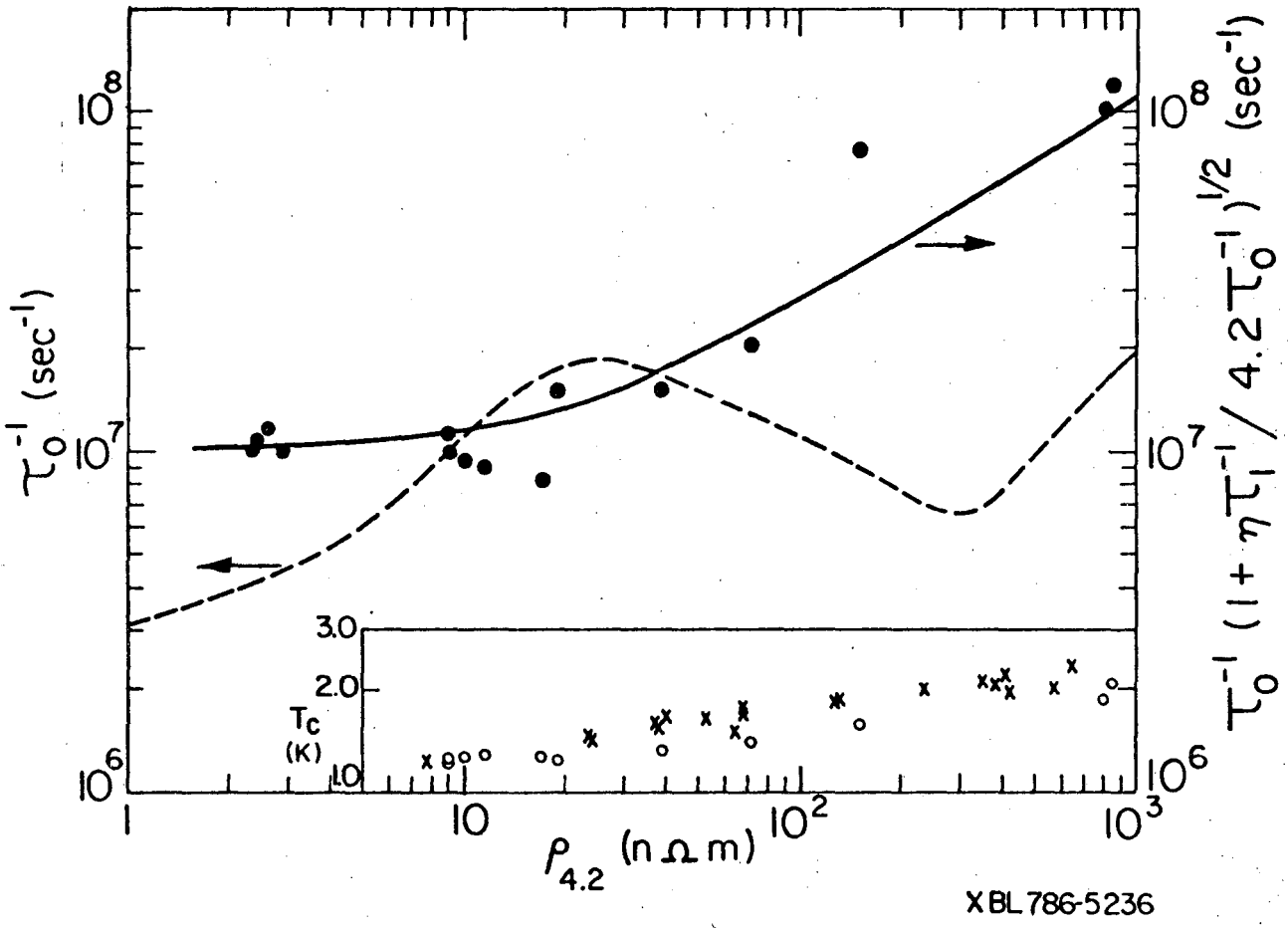
10^8
10^7
10^6
τ_0^{-1} (sec^{-1})
$\tau_0^{-1}(1+\eta\tau_1^{-1}/4.2\tau_0^{-1})^{1/2}$ (sec^{-1})
3.0
2.0
1.0
T_c (K)
1
10
10^2
10^3
$\rho_{4.2}$ (n Ω m)
XBL786-5236

Fig. 8

TECHNICAL INFORMATION DEPARTMENT
LAWRENCE BERKELEY LABORATORY
UNIVERSITY OF CALIFORNIA
BERKELEY, CALIFORNIA 94720